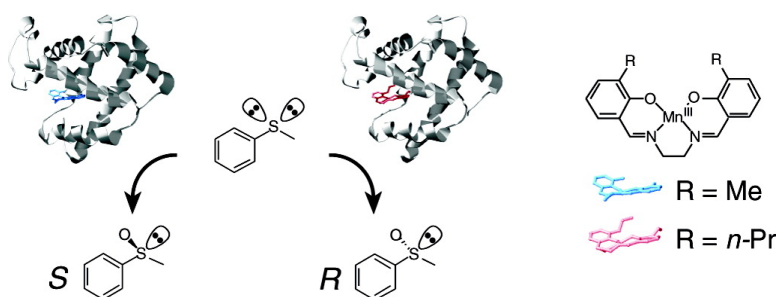Article

Coordinated Design of Cofactor and Active Site Structures in Development of New Protein Catalysts

Takafumi Ueno, Tomomi Koshiyama, Masataka Ohashi, Kazuyoshi Kondo,
Masaharu Kono, Atsuo Suzuki, Takashi Yamane, and Yoshihito Watanabe

More About This Article

Additional resources and features associated with this article are available within the HTML version:

- Supporting Information
- Links to the 3 articles that cite this article, as of the time of this article download
- Access to high resolution figures
- Links to articles and content related to this article
- Copyright permission to reproduce figures and/or text from this article

View the Full Text HTML

Coordinated Design of Cofactor and Active Site Structures in Development of New Protein Catalysts

Takafumi Ueno,[†] Tomomi Koshiyama,[‡] Masataka Ohashi,[§] Kazuyoshi Kondo,[||] Masaharu Kono,[||] Atsuo Suzuki,[||] Takashi Yamane,[||] and Yoshihito Watanabe*,[‡]

Contribution from the Research Center for Materials Science and Department of Chemistry, Graduate School of Science, Nagoya University, Nagoya 464-8602, Japan, Department of Structural Molecular Science, The Graduate University for Advanced Studies, Okazaki 444-8585, Japan, and Department of Biotechnology and Biomaterial, Graduate School of Engineering, Nagoya University, Nagoya 464-8602, Japan

Received July 6, 2004; Revised Manuscript Received February 18, 2005; E-mail: yoshi@nucc.cc.nagoya-u.ac.jp

Abstract: New methods for the synthesis of artificial metalloenzymes are important for the construction of novel biocatalysts and biomaterials. Recently, we reported new methodology for the synthesis of artificial metalloenzymes by reconstituting apo-myoglobin with metal complexes (Ohashi, M. et al., *Angew Chem., Int. Ed.* **2003**, *42*, 1005−1008). However, it has been difficult to improve their reactivity, since their crystal structures were not available. In this article, we report the crystal structures of M^{III}(Schiff base)·apo-A71GMbs (M = Cr and Mn). The structures suggest that the position of the metal complex in apo-Mb is regulated by (i) noncovalent interaction between the ligand and surrounding peptides and (ii) the ligation of the metal ion to proximal histidine (His93). In addition, it is proposed that specific interactions of Ile107 with 3- and 3′-substituent groups on the salen ligand control the location of the Schiff base ligand in the active site. On the basis of these results, we have successfully controlled the enantioselectivity in the sulfoxidation of thioanisole by changing the size of substituents at the 3 and 3′ positions. This is the first example of an enantioselective enzymatic reaction regulated by the design of metal complex in the protein active site.

Introduction

Design of proteins and enzymes for industrial and medical applications has been a long-standing goal in the field of protein chemistry. In the case of metalloenzymes, catalytic activity and stability of the native cofactors are regulated by specific interaction with amino acid residues in the protein cavities. If we could construct artificial metalloenzymes having high activity and selectivity, they can be used in the so-called "green process". While simple metal complexes have been used as cofactors in biocatalysts,[1] it is difficult to place them at the desired position in a protein matrix. Recently, the construction of new biocatalysts having high catalytic efficiency, selectivity, and stability has been reported.[2−13] One of the methods employed in these studies is the modification of native metal cofactors such as heme[14−16] and porphyrin derivatives.[17,18] Further, covalent bond formation of metal complexes with protein scaffolds or substrates has been attempted by using a cysteinyl thiol group or biotin, respectively.[4,19−25] For example, Whitesides and co-workers have reported asymmetric hydrogenation using the

[†] Research Center for Materials Science, Nagoya University.
[‡] Department of Chemistry, Nagoya University.
[§] The Graduate University for Advanced Studies.
[||] Department of Biotechnology and Biomaterial, Nagoya University.

(1) *Handbook of Metalloproteins*; Messerschmidt, A., Huber, R., Poulos, T., Wieghardt, K., Eds.; Wiley & Sons: New York, 2001; Vols. 1 and 2.
(2) Benson, D. E.; Wisz, M. S.; Hellinga, H. W. *Curr. Opin. Biochem.* **1998**, *9*, 370−376.
(3) Lu, Y.; Berry, S. M.; Pfister, T. D. *Chem. Rev.* **2001**, *101*, 3047−3080.
(4) Qi, D.; Tann, C.-M.; Haring, D.; Distefano, M. D. *Chem. Rev.* **2001**, *101*, 3081−3111.
(5) Hayashi, T.; Hisaeda, Y. *Acc. Chem. Res.* **2002**, *35*, 35−43.
(6) Velde, F. v. d.; Rantwijk, F. v.; Sheldon, R. A. *Trends Biotechnol.* **2001**, *19*, 73−80.
(7) Braha, O.; Walker, B.; Cheley, S.; Kasianowicz, J. J.; Song, L.; Gouaux, J. E.; Bayley, H. *Chem. Biol.* **1997**, *4*, 497−505.
(8) Hara, I.; Ueno, T.; Ozaki, S.; Itoh, S.; Lee, K.; Ueyama, N.; Watanabe, Y. *J. Biol. Chem.* **2001**, *276*, 36067−36070.
(9) Kato, S.; Yang, H.-J.; Ueno, T.; Ozaki, S.; Phillips, G. N., Jr.; Fukuzumi, S.; Watanabe, Y. *J. Am. Chem. Soc.* **2002**, *124*, 8506−8507.

(10) Miyawaki, A.; Llopis, J.; Heim, R.; McCaffery, J. M.; Adams, J. A.; Ikura, M.; Tsien, R. Y. *Nature* **1997**, *388*, 882−887.
(11) Pinto, A. L.; Hellinga, H. W.; Caradonna, J. P. *Proc. Natl. Acad. Sci. U.S.A.* **1997**, *94*, 5562−5567.
(12) Sigman, J. A.; Kwok, B. C.; Lu, Y. *J. Am. Chem. Soc.* **2000**, *122*, 8192−8196.
(13) Ueno, T.; Suzuki, M.; Goto, T.; Matsumoto, T.; Nagayama, K.; Watanabe, Y. *Angew. Chem., Int. Ed.* **2004**, *43*, 2527−2530.
(14) Hayashi, T.; Hitomi, Y.; Ando, T.; Mizutani, T.; Hisaeda, Y.; Kitagawa, S.; Ogoshi, H. *J. Am. Chem. Soc.* **1999**, *121*, 7747−7750.
(15) Hu, Y.-Z.; Tsukiji, S.; Shinkai, S.; Oishi, S.; Hamachi, I. *J. Am. Chem. Soc.* **2000**, *122*, 241−253.
(16) Monzani, E.; Alzuet, G.; Casella, L.; Redaelli, C.; Bassani, C.; Sanangelantoni, A. M.; Gullotti, M.; Gioia, L. D.; Santagostin, L.; Chillemi, F. *Biochemistry* **2000**, *39*, 9571−9582.
(17) Neya, S.; Funasaki, N.; Sato, T.; Igarashi, N.; Tanaka, N. *J. Biol. Chem.* **1993**, *268*, 8935−8942.
(18) Neya, S.; Tsubaki, M.; Hori, H.; Yonetani, T.; Funasaki, N. *Inorg. Chem.* **2001**, *40*, 1220−1225.
(19) Davies, R. R.; Distefano, M. D. *J. Am. Chem. Soc.* **1997**, *119*, 11643−11652.
(20) Ermacora, M. R.; Delfino, J. M.; Cuenoud, B.; Schepartz, A. *Proc. Natl. Acad. Sci. U.S.A.* **1992**, *89*, 6383−6387.
(21) Ma, S. K.; Lu, Y. *J. Inorg. Biochem.* **1999**, *74*, 217.
(22) Sigman, D. S.; Bruice, T. W.; Mazumder, A.; Sutton, C. L. *Acc. Chem. Res.* **1993**, *26*, 98−104.
(23) Lin, C.-C.; Lin, C.-W.; Chan, A. S. C. *Tetrahedron: Asymmetry* **1999**, *10*, 1887−1893.
(24) Wilson, M. E.; Whitesides, G. M. *J. Am. Chem. Soc.* **1978**, *100*, 306−307.
(25) Carey, J. R.; Ma, S. K.; Pfister, T. D.; Garner, D. K.; Kim, H. K.; Abramite, J. A.; Wang, Z. L.; Guo, Z. J.; Lu, Y. *J. Am. Chem. Soc.* **2004**, *126*, 10812−10813.

biotin-binding protein, avidin, as a chiral template for biotin–diphosphinerhodium(I) complexes.[24] To improve the enantioselectivity of the catalytic reactions, the biotinate ligands, avidin active site, and reaction conditions were optimized.[23,26] However, the reaction mechanism is still not clear due to limited structural information.

A few years ago, we reported a new method for the construction of artificial metalloenzymes,[27] starting with the removal of the heme prosthetic group from myoglobin (Mb), followed by insertion of a symmetric Cr[III] Schiff base complex, which is known as an oxidation catalyst in organic solvents,[28] into the empty cavity of apo-Mb. Unfortunately, they exhibit low reactivitiy and enantioselectivity in sulfoxidation of thioanisole.[27] Recently, we reconstituted apo-Mb and apo-A71GMb with Fe[III](3,3′-Me$_2$-salophen) (salophen = $N,N′$-bis(salicylidene)-1,2-phenilenediamine) (**1**), and their crystal structures were successfully determined.[29] While the crystal structure of Fe·**1**·apo-A71GMb shows tight binding of the salophen complex in the apo-A71GMb cavity, the Schiff base ligand **1** in Fe·**1**·apo-Mb is highly disordered due to steric repulsion of **1** for the side chain of Ala71 in the active site of wild-type apo-Mb. In addition, the structure of Fe·**1**·apo-A71GMb suggests possible accommodation of small substrates in the cavity. In fact, the cyanide association rate constant of Fe·**1**·apo-A71GMb is 215-fold larger compared to that of Fe·**1**·apo-Mb. The crystal structures also suggest that the position of the metal complex could be affected by noncovalent interaction between the ligand and surrounding peptides. On the basis of these results, we report the molecular design of M[III](Schiff base)·apo-Mbs (M = Cr and Mn) for the regulation of the enantioselectivity in the thioanisole oxidation by adjusting the position of a Schiff base complex in the active site. This is the first example of the rational design of artificial metalloenzymes based on structural information.

3,3'-Me$_2$-Salophen (**1**)

3,3'-R$_2$-Salen
R = Me (**2**), Et (**3**), *n*-Pr (**4**)
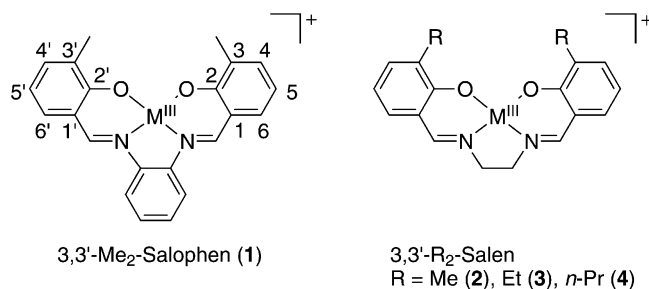
Results and Discussion

Preparation of M(Schiff Base)·apo-Mbs (M = Cr and Mn). Cr[III](Schiff base)·apo-Mbs and Mn[III](Schiff base)·apo-Mbs were synthesized according to a reported procedure.[27] Cr·**1**·apo-A71GMb and Mn·**1**·apo-A71GMb were crystallized, and their crystal structure was determined as described below. On the other hand, Mn(salophen)·apo-H64D/A71GMb could not be purified by a Sephadex G-50 size-exclusion column due to the dissociation of Mn(salophen) from apo-H64D/A71GMb. The results suggest that the stability of the composites highly depends

(26) Collot, J.; Gradinaru, J.; Humbert, N.; Skander, M.; Zocchi, A.; Ward, T. R. *J. Am. Chem. Soc.* **2003**, *125*, 9030–9031.
(27) Ohashi, M.; Koshiyama, T.; Ueno, T.; Yanase, M.; Fujii, H.; Watanabe, Y. *Angew. Chem., Int. Ed.* **2003**, *42*, 1005–1008.
(28) Srinivasan, K.; Kochi, J. K. *Inorg. Chem.* **1985**, *24*, 4671–4679.
(29) Ueno, T.; Ohashi, M.; Kono, M.; Kondo, K.; Suzuki, A.; Yamane, T.; Watanabe, Y. *Inorg. Chem.* **2004**, *43*, 2852–2858.

Table 1. Summary of X-ray Data from the Crystals of Cr·**1**·apo-A71GMb and Mn·**1**·apo-A71GMb

	Cr·**1**·apo-A71GMb	Mn·**1**·apo-A71GMb
Crystallographic Statistics		
space group	$P2_12_12_1$	$P2_12_12_1$
unit cell (Å)		
a, b, c	33.0, 58.8, 76.2	33.3, 57.8, 75.4
resolution (Å)^a	40.0–1.45	40.0–1.45
	(1.50–1.45)	(1.50–1.45)
total observations	391885	359451
unique reflections	26426	25409
completeness (%)^a	97.1 (90.0)	95.4 (84.7)
R_{merge} (%)^{a,b}	9.3 (26.0)	5.9 (26.1)
$I/\sigma(I)^a$	40.6 (9.9)	37.3 (5.8)
molecules per asymmetric unit	1	1
Refinement Statistics		
resolution (Å)	30.3–1.45	27.0–1.45
number of reflections		
working set/test set	24604/1251	23524/1207
R-factor (%)^c	19.4	20.6
R_{free} (%)^d	21.9	21.8
rmsd		
bonds (Å)	0.004	0.004
angles (deg)	1.8	1.8
dihedrals (deg)	17.6	17.1
improper (deg)	0.69	0.68
Ramachandran plot (%)^e		
most favored	92.5	90.5
allowed	7.5	9.5
final model		
No. of residues	152 (0–95, 98–153)	154
No. of M[III](3,3′-Me$_2$-salophen)	1	1
No. of water molecules	267	209
No. of phosphate ions	6	6

^{a} Values in parentheses are for the highest resolution shell. ^{b} R_{merge} = $\sum|I - \langle I\rangle|/\sum I$, where I is the integrated intensity of a given reflection. ^{c} R = $\sum||F_o| - |F_c||/\sum|F_o|$, where F_o and F_c are the observed and calculated structure factor amplitudes, respectively. ^{d} R_{free}: an R factor calculated on a partial set that is not used in the refinement of the structure. ^{e} Ramachandran plot parameters were calculated using PROCHECK.[39]

on the hydrophobic interaction between 3- and 3′-substituents and amino acids in the active site rather than the ligation of Mn atom to His93. On the other hand, the replacement of the phenylenediamine unit in salophen with ethylenediamine did not influence its affinity. The binding constants of Cr·**1** or Mn·**1** to apo-A71GMb could not be obtained since the UV–vis spectral changes of apo-A71GMb upon the addition of Cr·**1** or Mn·**1** did not show clear isosbestic points. This can be attributed to multiple or complicated binding pathways of the complexes to apo-A71G.

Crystal Structures of Cr·1·apo-A71GMb and Mn·1·apo-A71GMb. The crystallizations of Cr·**1**·apo-A71GMb and Mn·**1**·apo-A71GMb were carried out as described previously.[27,30] Their structures were refined to 1.45 Å resolution. The *R*-factors for Cr·**1**·apo-A71GMb and Mn·**1**·apo-A71GMb were 19.4 and 20.6%, respectively. The final refinement statistics are presented in Table 1. Superimposed structures of Mn·**1**·apo-A71GMb and met-Mb are shown in Figure 1a. The deviation of the C$^\alpha$ positions in Mn·**1**·apo-A71GMb from met-Mb is 0.77 Å. The value is similar to those reported for Fe(III)porphyrin·apo-Mb (0.77 Å) and biliverdin·apo-Mb (0.60 Å).[17,30] Small tertiary structure deviation from met-Mb suggests that apo-Mb is capable of including non-native prosthetic groups in the heme cavity without serious structural perturbation, if the metal complex is

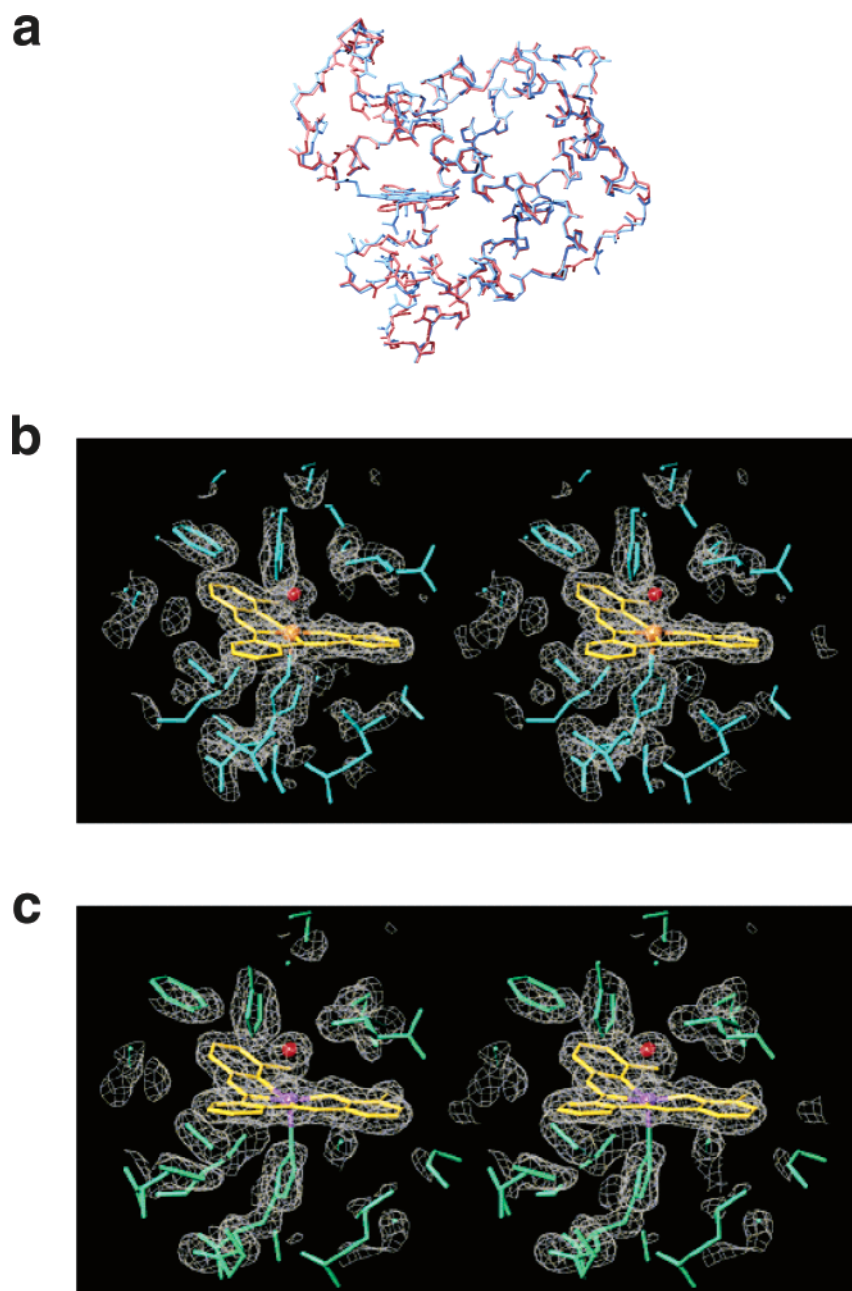(30) Wagner, U. G.; Muller, N.; Schmitzberger, W.; Falk, H.; Kratky, C. *J. Mol. Biol.* **1995**, *247*, 326–337.

Figure 1. Crystal structures of M·**1**·apo-A71GMb (M = Mn and Cr). (a) Whole structure of Mn·**1**·apo-A71GMb (red) superimposed on met-Mb (blue).[38] (b) Stereo diagrams showing the active site structures of Cr·**1**·apo-A71GMb. (c) Mn·**1**·apo-A71GMb.

designed properly. As shown in Figure 1b, Cr·**1** is fixed in the heme cavity by ligating the chromium atom to His93 with a Cr—N distance of 2.13 Å. The distance is comparable to 2.07 and 2.17 Å of [Cr^{III}(salen)(3-Me-Im)$_2$]$^+$.[31] A water molecule tightly ligates to the Cr atom at a distance of 2.00 Å, similar to those of [Cr^{III}(salen)(H_2O)$_2$]$^+$ (Figure 1b and Table 2).[32] While Mn·**1** exhibits longer bond distances with His93 and H_2O compared to those of Cr·**1**·apo-A71GMb (Table 2), the bond distances are similar to those of [Mn^{III}(7,7′-Ph$_2$-salen)(Py)$_2$]$^+$ and [Mn^{III}(3,3′-OMe$_2$-salen)(H_2O)$_2$]$^+$ (Table 2).[33,34]

(31) Matsumoto, N.; Inoue, K.; Okawa, H.; Kida, S. *Chem. Lett.* **1989**, 1251–1254.
(32) Coggon, P.; Mcphail, A. T.; Mabbs, P. E.; Richards, A.; Thornley, A. S. *J. Chem. Soc. A* **1970**, 3296–3303.
(33) Srinivasan, K.; Michaud, P.; Kochi, J. K. *J. Am. Chem. Soc.* **1986**, *108*, 2309–2320.

Table 2. Selected Distances of Metal–O (H_2O) and Metal–N$^\epsilon$ (His93) in M·**1**·apo-A71GMbs (M = Cr and Mn) and the Related Metal Complexes

	metal–N$^\epsilon$	metal–O
Cr·**1**·apo-A71GMb	2.13	2.00
[Cr^{III}(salen)(3-Me-Im)$_2$]$^{+a}$	2.07, 2.17	–
[Cr^{III}(salen)(H_2O)$_2$]$^{+b}$	–	1.92, 2.09
Mn·**1**·apo-A71GMb	2.40	2.38
[Mn^{III}(7,7′-Ph$_2$-salen)(Py)$_2$]$^{+c}$	2.35, 2.35	–
[Mn^{III}(3,3′-OMe$_2$-salen)(H_2O)$_2$]$^{+d}$	–	2.25, 2.38

^{a} Reference 31. ^{b} Reference 32. ^{c} Reference 33. ^{d} Reference 34.

Mn·**1** makes a number of hydrophobic interactions with the surrounding amino acids as shown in Figure 2a. The benzene

(34) Zhang, C. G.; Tian, G. H.; Ma, Z. F.; Yan, D. Y. *Transition Met. Chem.* **2000**, *25*, 270–273.
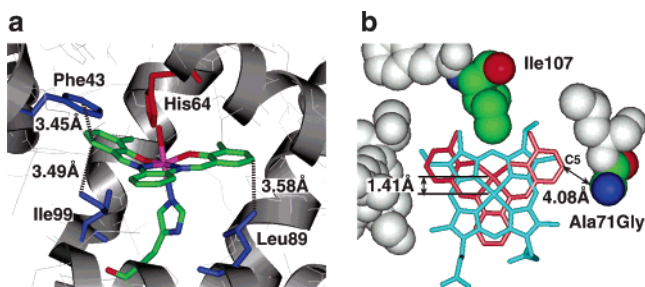
Figure 2. Active site structure of Mn·**1**·apo-A71GMb: (a) side and (b) top views. The heme of met-Mb[38] (blue) is superimposed on Mn·**1**·apo-A71GMb in (b).

ring of Mn·**1** in apo-A71GMb shows an aromatic/aromatic interaction with the Phe43 side chain (closest contact is 3.45 Å).[35] Further, the side chains of Leu89 and Ile99 also interact with **1** through C–H/π interactions at distances of 3.58 and 3.49 Å, respectively (Figure 2a).[36] Thus, a large part of stability of the composite is provided by noncovalent interaction as reported for met-Mb.[37]

Figure 2b shows superimposed active site structures of Mn·**1**·apo-A71GMb and met-Mb. The Mn atom is located much deeper inside the protein (1.41 Å) compared to the heme iron in the active site. The vinyl and methyl groups at the 2- and 3-positions of the heme show hydrophobic interaction with Ile107 to control the penetration depth of the heme in the pocket.[38] In fact, porphyrin and biliverdin ligands, which do not make specific interaction with Ile107, are inserted deeper in the heme pocket than the heme in met-Mb.[17,30] In the case of Mn·**1**·apo-A71GMb, the two methyl groups at the 3- and 3′-positions in **1** also interact with hydrophobic Ile107 (Figure 2b) to allow the Mn complex to be held deeper in the pocket than the heme, and consequently, the C$^\alpha$ atom of Gly71 in the mutant locates close to the C5 atom of the Schiff base ligand (4.08 Å). As reported before, the crystal structure of Fe·**1**·apo-A71GMb showed the tight binding of the complex in the Mb cavity, while the Fe·**1** in Fe·**1**·apo-Mb is highly disordered due to the steric hindrance between the C5 and the side chain of Ala71.[29] Thus, it is clear that the 3- and 3′-methyl groups and Ala71Gly mutation regulate the stability, penetration depth, and orientation of **1** in the heme cavity.

Crystal Structure-Based Molecular Design of Schiff Base Complexes and apo-Mb Mutants. To improve the catalytic reactivity, Schiff base ligands **2**−**4** were designed on the basis of the crystal structures. It is known that the accessibility of substrates is limited by the steric hindrance of heme and His64.[40] The crystal structure of Mn·**1**·apo-A71GMb shows a narrow channel between His64 and the phenylenediamine unit of **1** (Figure 2a). Thus, the phenylenediamine unit was substituted by an ethylenediamine unit to enlarge the active site of Mn·**1**·apo-A71GMb. The position of the metal complex in the active site is an important factor to determine the reaction selectivity.

(35) Hunter, C. A.; Lawson, K. R.; Perkins, J.; Urch, C. J. *J. Chem. Soc., Perkin Trans. 2* **2001**, 651−669.
(36) Nishio, M.; Hirota, M.; Umezawa, Y. *The CH/π Interaction: Evidence, Nature, and Consequences*; WILEY-VCH: New York, 1998.
(37) Hunter, C. L.; Lloyd, E.; Eltis, L. D.; Rafferty, S. P.; Lee, H.; Smith, M.; Mauk, A. G. *Biochemistry* **1997**, *36*, 1010−1017.
(38) Takano, T. *J. Mol. Biol.* **1977**, *110*, 537−568.
(39) Laskowski, R. A.; MacArthur, M. W.; Moss, D. S.; Thornton, J. M. *J. Appl. Crystallogr.* **1993**, *26*, 283−291.
(40) Yang, H.-J.; Matsui, T.; Ozaki, S.; Kato, S.; Ueno, T.; Phillips, G. N., Jr.; Fukuzumi, S.; Watanabe, Y. *Biochemistry* **2003**, *42*, 10174−10181.
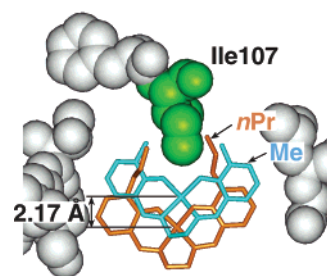

Figure 3. Calculated active site structure of Mn·**2**·apo-H64D/A71GMb superimposed on Mn·**4**·apo-H64D/A71GMb. The calculations were performed with InsightII/Discover 3 using the ESFF force field.

Table 3. Enantioselective Thioanisole Sulfoxidation[a]

catalyst	rate[b]	% ee
Cr·(salophen)·apo-H64D/A71GMb	83 ± 3	8 ± 0.5 (S)
Cr·**1**·apo-A71GMb	22 ± 3	5 ± 0.2 (S)
Cr·**1**·apo-H64D/A71GMb	130 ± 6	30 ± 1.1 (S)
Cr·**2**·apo-H64D/A71GMb	210 ± 76	33 ± 1.6 (S)
Cr·**3**·apo-H64D/A71GMb	48 ± 1	14 ± 0.2 (S)
Cr·**4**·apo-H64D/A71GMb	43 ± 4	12 ± 0.1 (S)
Mn·**2**·apo-A71GMb	1295 ± 119	17 ± 0.6 (R)
Mn·**3**·apo-A71GMb	803 ± 5	23 ± 0.2 (R)
Mn·**4**·apo-A71GMb	2724 ± 69	27 ± 0.1 (R)
Mn·**1**·apo-H64D/A71GMb	158 ± 8	23 ± 0.5 (S)
Mn·**2**·apo-H64D/A71GMb	464 ± 62	32 ± 0.1 (S)
Mn·**3**·apo-H64D/A71GMb	135 ± 5	5 ± 0.7 (S)
Mn·**4**·apo-H64D/A71GMb	180 ± 7	13 ± 0.5 (R)
Mn·**2** in buffer	62 ± 3	0
Mn·**3** in buffer	39 ± 6	0
Mn·**4** in buffer	87 ± 6	0

[a] Sulfoxidation was carried out in sodium acetate buffer (50 mM, pH 5.0) at 35 °C in the presence of a Mb composite (10 μM), thioanisole (1 mM), and H_2O_2 (1 mM). [b] The unit of the rate is 10^{-3} turnover min^{-1}.

The position of Mn·**1** in apo-A71GMb was regulated by several types of interactions, especially the hydrophobic interaction between Ile107 and the 3- and 3′-methyl groups of **1**. Thus, the two methyl groups were substituted either by ethyl or by *n*-propyl groups to regulate the penetration depth of Mn(Schiff base) complexes in the protein. Energy minimization of the composites suggests that the Mn atoms are exposed to the outside of the cavity by 0.83 and 2.17 Å as compared to that of Mn·**2** (Figure 3) due to the Et and *n*-Pr substitutions, respectively.

Apo-H64D/A71GMb and apo-A71GMb were reconstituted with Mn and Cr Schiff base complexes for asymmetric sulfoxidation with H_2O_2. The crystal structure of H64D/V68AMb shows that the distal cavity is enlarged by the H64D mutation and the substrates could easily access the active site.[40,41] The replacement of Ala71 to Gly reduces the steric hindrance between the Schiff base ligand and the amino acid at position 71 (Figure 2b).

Reactivity of Schiff Base Complexes in apo-Mb Cavity. The H_2O_2-dependent sulfoxidations of thioanisole were examined at 35 °C (50 mM sodium acetate buffer, pH 5.0), and the results of the sulfoxidation are listed in Table 3. The oxidation rates by Cr and Mn Schiff base complexes are accelerated by inserting them in apo-Mb. Cr·**2**·apo-H64D/A71GMb and Cr-(5,5′-*t*-Bu₂-salophen)·apo-H64D/A71GMb exhibit 15- and 6-fold higher activities than that of Cr(5,5′-*t*-Bu₂-salophen) in buffer, respectively.[27] Further, Mn(salen derivative)·apo-A71GMbs

(41) Matsui, T.; Ozaki, S.; Watanabe, Y. *J. Am. Chem. Soc.* **1999**, *121*, 9952−9957.

show 21−31-fold increased rates compared to those of Mn-(salen derivative) in the same buffer solution (Table 3). The Mn and Cr Schiff base complexes are known to catalyze the sulfoxidation of thioethers through the oxo transfer from $Mn^V=O$ and $Cr^V=O$, respectively.[42,43] Kochi et al. have studied the catalytic oxidation by chromium Schiff base complexes in acetonitrile and observed the enhancement of the catalytic reactivity by the addition of neutral donor ligand, such as pyridine and pyridine *N*-oxide.[28,44] The axial ligation is expected to weaken the $Cr^V=O$ bond, which accounts for the increased reactivity of the six-coordinate oxochromium(V) cation.[44] We have previously confirmed the formation of oxochromium(V) cation in Cr(5,5′-*t*-Bu₂-salophen)·apo-H64D/A71GMb.[27] The oxochromium(V) cation could be activated by the axial ligation of His93 to the Cr atom in the hydrophobic cavity (Figure 1). Mn(Schiff base) complexes also require donor ligands such as imidazole to stabilize the highly reactive $Mn^V=O$ (salen) species formed by the addition of H_2O_2 and to accelerate the rate of oxidation.[45] These results indicate that the imidazole ligation (His93) to the Cr and Mn atoms efficiently activates the $M^V=O$ bond in the active site, although a large excess of the donor ligands is required in the salen-catalyzed oxidation in organic solvents.[44,46]

In addition, we attempted to design a ligand with an enlarged cavity size by replacing **1** with **2** to increase the accessibility of substrates. The rate with Mn·**2**·apo-H64D/A71GMb is 3-fold higher than that with Mn·**1**·apo-H64D/A71GMb (Table 3).

Asymmetric Sulfoxidation. Modification of Schiff base ligands also affects the enantioselectivity in sulfoxidation as shown in Table 3. The % ee by Cr·**1**·apo-H64D/A71GMb is 6-fold greater than that of Cr·**1**·apo-A71GMb. The result suggests that thioanisole reacts with Cr·**1** in the chiral cavity enlarged by the replacement of His64 to Asp. In the case of apo-H64D/A71GMb, Cr·**1** shows 4- and 2-fold increased % ee values compared to those of Cr(salophen) and Cr(5,5′-*t*-Bu₂-salophen), respectively.[27] The replacement of **1** with **2** also improves enantioselectivity for both of the Cr and Mn complexes in apo-Mb active sites. With respect to the substituents at 3- and 3′-positions of the salen ligand of Cr(Schiff base)·apo-H64D/A71GMb, bulkier substituents increase a relative amount of the *R*-isomer (i.e., 33 (*S*) for **2**, 14 (*S*) for **3**, and 12 (*S*) for **4**).

Proposed Mechanism for the Enantioselective Sulfoxidation. The crystal structure of Mn·**1**·apo-A71GMb shows hydrophobic interaction between the 3- and 3′-methyl groups and Ile107 (Figure 2b). The replacement of the methyl groups with bulky ethyl and *n*-propyl groups is expected to change the position of the metal ion. Molecular modeling calculations of Mn(3,3′-X₂-salen)·apo-H64D/A71GMbs (X = Me, Et, and *n*-Pr) indicate that the Mn atoms of Mn·**3** and Mn·**4** in the protein are located 0.83 and 2.17 Å from the position of Mn·**2**, respectively (Figure 3). In addition, the calculation suggests that the position of thioanisole in the three composites is not changed
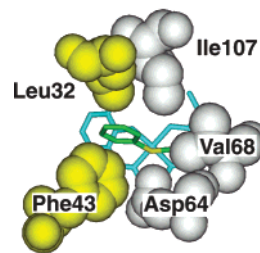
(42) Palucki, M.; Hanson, P.; Jacobsen, E. N. *Tetrahedron Lett.* **1992**, *33*, 7111−7114.
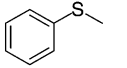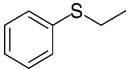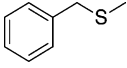(43) Venkataramanan, N. S.; Premsingh, S.; Rajagopal, S.; Pitchumani, K. *J. Org. Chem.* **2003**, *68*, 7460−7470.
(44) Samsel, E. G.; Srinivasan, K.; Kochi, J. K. *J. Am. Chem. Soc.* **1985**, *107*, 7606−7617.
(45) Berkessel, A.; Frauenkron, M.; Schwenkreis, T.; Steinmetz, A.; Baum, G.; Fenske, D. *J. Mol. Catal. A* **1996**, *113*, 321−342.
(46) Srinivasan, K.; Michaud, P.; Kochi, J. K. *J. Am. Chem. Soc.* **1986**, *108*, 2309−2320.

Figure 4. Proposed binding structure of thioanisole in Mn·**2**·apo-H64D/A71GMb.

Scheme 1. Schematic Drawing for the Regulation Mechanism of Enantioselective Thioanisole Sulfoxidation Catalyzed by Mn(3,3′-X₂-salen)·apo-H64D/A71GMbs (X = Me, Et, and *n*-Pr)
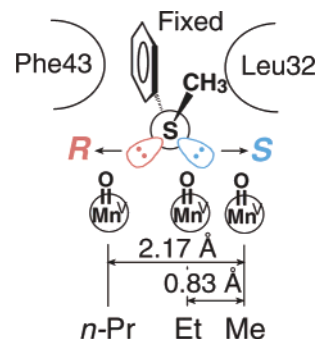
since the replacement of two methyl groups with Et or *n*-Pr does not affect the interaction of the phenyl group in thioanisole with Phe43 and Leu32 (Figure 4). These considerations indicate that the relative position of the sulfur atom and the oxo−metal center could be altered as shown in Scheme 1, resulting in the change of enantioselectivity in the sulfoxidation. In fact, bulkier substituents in Cr·apo-H64D/A71GMb's increase a relative amount of the *R*-isomer (Table 3).

To prove these ideas, the % ee values of the thioanisole oxidation catalyzed by a series of Mn·**2**·apo-H64D/A71GMb, Mn·**3**·apo-H64D/A71GMb, and Mn·**4**·apo-H64D/A71GMb were evaluated (Table 3). While Mn·**2**·apo-H64D/A71GMb showed 32% ee (*S*) selectivity, introduction of bulkier groups at the 3,3′-positions induces relative *R*-selectivity to end up with 13% (*R*) for **4**. The series of Cr(3,3′-X₂-salen)·apo-H64D/A71GMb and Mn(3,3′-X₂-salen)·apo-H64D/A71GMb (X = Me, Et, and *n*-Pr) show the same trend in enantioselective sulfoxidation (Table 3). In addition, the same shift of the selectivity is observed in the phenyl ethyl sulfide oxidation (Table 4). Interestingly, the *R*-selectivity in the oxidation of benzyl methyl sulfide was not affected by the introduction of bulkier groups. This is because the sulfur atom in benzyl methyl sulfide is free to move even though the phenyl group is fixed by its interaction with Phe43 and Leu32 (Table 4). The enantioselectivity in the sulfoxidation of 2-methyl, 2,4-dimethyl, and 2,6-dimethyl thioanilsoles catalyzed by Mn·**2**·apo-H64D/A71GMb is less than that of thioanisole (below 8% ee). This can be attributed to the inability of the substrates to bind to the site for thioanisole due to their steric hindrance. *These results also supported our idea that the enantioselectivity of catalytic reactions in protein cavities can be regulated by the positions of a metal center and substrate.*

In summary, we have determined the X-ray crystal structures of Cr·**1**·apo-A71GMb and Mn·**1**·apo-A71GMb and provided the structural insight for the catalytic activity and enantiose-

Table 4. Enantiospecific Sulfoxidation of Various Sulfides by Mn(salen derivative)·apo-H64D/A71GMb

	Mn·**2**		Mn·**3**		Mn·**4**	
	rate[a]	(% ee)	rate[a]	(% ee)	rate[a]	(% ee)
	464 ± 62	32 ± 0.1 (S)	135 ± 5	5 ± 0.7 (S)	180 ± 7	13 ± 0.5 (R)
	117 ± 16	22 ± 1.0 (S)	82 ± 2	16 ± 1.0 (S)	176 ± 8	4 ± 0.5 (S)
	465 ± 57	12 ± 0.5 (R)	412 ± 109	8 ± 0.9 (R)	369 ± 27	13 ± 0.3 (R)

^{a} The unit of the rate is 10^{-3} turnover min^{-1}.

lectivity. The catalytic reactivity has been improved by modifying the Schiff base ligands. Importantly, the idea of the enantioselectivity being regulated by the position of the inserted synthetic metal complex has been experimentally proved. The results clearly show the potential of this method for the design of artificial metalloenzymes for the synthesis of new biocatalysts and biomaterials. Further structure-based ligand and protein design are currently in progress to improve the reactivity and selectivity of the artificial metalloenzymes.

Experimental Section

Materials. Reagents were purchased from TCI, Wako, Nacalai Tesque, and Sigma-Aldrich and used without further purification. Mb mutant genes were constructed by cassette mutagenesis. The expression and purification of the mutants were performed as reported previously.[47]

Preparation of Schiff Base Ligands. 3-Ethyl-salicylaldehyde, 3-*n*-propylsalicylaldehyde, and Schiff base ligands were prepared by literature methods.[48,49] Ethylenediamine (0.06 g, 1 mmol) was added to an ethanol solution of 2-hydroxy-3-methyl-benzaldehyde (0.27 g, 2 mmol). This mixture was refluxed for 2.5 h. The resulting precipitate was collected by filtration and dried under vacuum to give *N,N'*-bis-(3-methylsalicylidene)-1,2-ethylenediamine (3,3′-Me₂-salen-H₂) as yellow microcrystals. 3,3′-Me₂-salen-H₂ (**2**): Yield 87%, Anal. Calcd for $C_{18}H_{20}N_2O_2$: C, 72.95; H, 6.80; N, 9.45. Found: C, 72.93; H, 6.96; N, 9.48. ESI-TOF MS *m/z*: [**2** + H]⁺ 297.0 (calcd 297.1). The other Schiff base ligands (**3**, **4**) were prepared by the same procedure. 3,3′-Et₂-salen-H₂ (**3**): Yield 4%, Anal. Calcd for $C_{20}H_{24}N_2O_2 \cdot 0.25H_2O$: C, 73.03; H, 7.51; N, 8.52. Found: C, 72.67; H, 7.84; N, 8.68. ESI-TOF MS *m/z*: [**3** + H]⁺ 325.0 (calcd 325.1). 3,3′-*n*-Pr₂-salen-H₂ (**4**): Yield 42%, Anal. Calcd for $C_{22}H_{28}N_2O_2 \cdot 0.25H_2O$: C, 74.02; H, 8.05; N, 7.85. Found: C, 73.88; H, 8.07; N, 7.80. ESI-TOF MS *m/z*: [**4**+H]⁺ 353.1 (calcd 353.2). The ligand of 3,3′-Me₂-salophen-H₂ (**1**) was synthesized by the reported method.[27] 3,3′-Me₂-salophen-H₂ (**1**): Yield 80%, ESI-TOF MS *m/z*: 345.1 (calcd 344.1).

Preparation of Mn(III) Schiff Base Complexes. Mn(III) Schiff base complexes were prepared by a literature method.[49] To an ethanol (13 mL) solution of **2** (0.10 g, 0.33 mmol) was added MnCl₂·4H₂O (0.20 g, 1.0 mmol). The mixture was refluxed at 85 °C for 2.5 h, and then the precipitate was removed by Celite filtration. The solution was concentrated by a rotary evaporation. The resulting precipitate was collected by filtration and dried under vacuum to give [Mn·**2**]Cl as black microcrystals. [Mn·**2**]Cl: Yield 63%, Anal. Calcd for $C_{18}H_{18}N_2O_2$-MnCl·2.5H₂O: C, 50.30; H, 5.39; N, 6.52. Found: C, 50.57; H, 5.28; N, 6.82. ESI-TOF MS *m/z* : [Mn·**2**]⁺ 349.1 (calcd 349.0). The other Mn(III) complexes were prepared by the same procedure. [Mn·**3**]Cl: Yield 37%, Anal. Calcd for $C_{20}H_{22}N_2O_2$MnCl: C, 58.19; H, 5.37; N,

6.79. Found: C, 58.47; H, 4.97; N, 6.27. ESI-TOF MS *m/z*: [Mn·**3**]⁺ 377.0 (calcd 377.1). [Mn·**4**]Cl: Yield 36%, Anal. Calcd for $C_{22}H_{26}N_2O_2$-MnCl: C, 59.94; H, 5.94; N, 6.35. Found: C, 60.02; H, 5.95; N, 6.19. ESI-TOF MS *m/z*: [Mn·**4**]⁺ 404.9 (calcd 405.1). [Mn·**1**]Cl: Yield 58%, ESI-TOF MS *m/z* : [Mn·**1**]⁺ 396.9 (calcd 397.0).

Preparation of Cr(III) Schiff Base Complexes. Cr(III) Schiff base complexes were prepared by a literature method.[27] [Cr·**1**]BF₄: Anal. Calcd for $C_{22}H_{18}BF_4N_2O_2Cl \cdot 2.75H_2O$: C, 49.79; H, 4.46; N, 5.28. Found: C, 49.69; H, 4.62; N, 5.45. ESI-TOF MS *m/z*: [Cr·**1**]⁺·(CH₃-CN)₂ 476.0 (calcd 476.1). [Cr·**2**]BF₄: ESI-TOF MS *m/z*: [Cr·**2**]⁺·(CH₃-CN)₂ 428.0 (calcd 428.1). [Cr·**3**]BF₄: ESI-TOF MS *m/z*: [Cr·**3**]⁺ 374.1 (calcd 374.1). [Cr·**4**]BF₄: ESI-TOF MS *m/z*: [Cr·**4**]⁺ 402.2 (calcd 402.1).

Reconstitution of Mn(III)(Schiff base)·apo-Mb. The reconstitution of apo-Mb with Mn(III)(Schiff base) was carried out by applying a method of modified hemes. [Mn·**2**]Cl dissolved in MeOH (1.5 equiv, 3 mM) was added dropwise to an apo-H64D/A71GMb solution (0.2 mM, 17.5 mL) in 10 mM Tris/HCl buffer (pH 7.0). The mixture was dialyzed against 10 mM Bis-Tris/HCl buffer (pH 6.0) for 6 h and then loaded on Sephadex G-25 equilibrated with 10 mM Tris/HCl buffer (pH 7.0). The resulting solution was finally purified by size-exclusion column (Sephadex G-50) equilibrated with 10 mM Tris/HCl buffer (pH 7.0). Mn·**2**·apo-H64D/A71GMb: Yield 2%, ESI-TOF MS: 17643.2 (calcd 17 643.0), UV–vis (10 mM Tris/HCl buffer, pH 7.0) λ/nm (ε/ M⁻¹ cm⁻¹): 281.5 (370 300), 317 (33 600), 401.5 (12 200). The other Mn(III)(Schiff base)·apo-Mbs were prepared by the same procedure. Mn·**3**·apo-H64D/A71GMb: Yield 17%, ESI-TOF MS: 17 669.6 (calcd 17671.1), UV−vis (10 mM Tris/HCl buffer, pH 7.0) λ/nm (ε/M⁻¹ cm⁻¹): 281.5 (49 800), 314.5 (17 400), 403 (5900). Mn·**4**·apo-H64D/ A71GMb: Yield 15%, ESI-TOF MS: 17698.5 (calcd 17 699.1), UV− vis (10 mM Tris/HCl buffer, pH 7.0) λ/nm (ε/M⁻¹ cm⁻¹): 282.5 (77 100), 314 (31 300), 411 (9900). Mn·**1**·apo-H64D/A71GMb: Yield 4%, ESI-TOF MS: 17 691.8 (calcd 17691.0), UV−vis (10 mM Tris/ HCl buffer, pH 7.0) λ/nm (ε/M⁻¹ cm⁻¹): 282.5 (236 800), 318.5 (102 200), 333 (99 100), 446.5 (10 500). Mn·**2**·apo-A71GMb: Yield 0.7%, UV−vis (10 mM Tris/HCl buffer, pH 7.0) λ/nm (ε/M⁻¹ cm⁻¹): 280.5 (1 165 000), 403.5 (18 570). Mn·**3**·apo-A71GMb: Yield 17%, ESI-TOF MS: 17 692.2 (calcd 17693.2), UV−vis (10 mM Tris/HCl buffer, pH 7.0) λ/nm (ε/M⁻¹ cm⁻¹): 281.5 (15 100), 314.4 (5066), 413.0 (1820). Mn·**4**·apo-A71GMb: Yield 5%, ESI-TOF MS: 17 720.5 (calcd 17 721.2), UV−vis (10 mM Tris/HCl buffer, pH 7.0) λ/nm (ε/M⁻¹ cm⁻¹): 282.0 (62 830), 316.8 (24 720), 414.5 (8680).

Reconstitution of Cr(III)(Schiff base)·apo-Mb. [Cr·**1**]BF₄ dissolved in MeOH (1.5 equiv, 2.6 mM) was added dropwise to an apo-H64D/A71GMb solution (0.18 mM, 16 mL) in 10 mM Tris/HCl buffer (pH 7.0). The mixture was dialyzed against 10 mM Bis-Tris/HCl buffer (pH 6.0) for 6 h and then loaded on Sephadex G-25 equilibrated with 10 mM Tris/HCl buffer (pH 7.0). The resulting solution was finally purified by size-exclusion column (Sephadex G-50) equilibrated with 10 mM Tris/HCl buffer (pH 7.0). Cr·**1**·apo-H64D/A71GMb: Yield 5%, ESI-TOF MS: 17 687.7 (calcd 17 688.0), UV−vis (10 mM Tris/HCl

(47) Springer, B. A.; Egeberg, K. D.; Sligar, S. G.; Rohlfs, R. J.; Mathews, A. J.; Olson, J. S. *J. Biol. Chem.* **1989**, *264*, 3057−3060.
(48) Hofslokken, N. U.; Skattebol, L. *Acta Chem. Scand.* **1999**, *53*, 258−262.
(49) Ciringh, Y.; Gordon-Wylie, S. W.; Norman, R. E.; Clark, G. R.; Weintraub, S. T.; Horwitz, C. P. *Inorg. Chem.* **1997**, *36*, 4968−4982.

buffer, pH 7.0) λ/nm (ϵ/M^{-1} cm^{-1}): 282 (69 800), 342.5 (35 700), 473.5 (12 600). Cr·**2**·apo-H64D/A71GMb: Yield 3%, ESI-TOF MS: 17 638.8 (calcd 17 640.0), UV−vis (10 mM Tris/HCl buffer, pH 7.0) λ/nm (ϵ/ M^{-1} cm^{-1}): 281.5 (231 300), 414.5 (6600). Cr·**3**·apo-H64D/A71GMb: Yield 4.5%, UV−vis (10 mM Tris/HCl buffer, pH 7.0) λ/nm (ϵ/M^{-1} cm^{-1}): 280.5 (197 900), 402.5 (5980). Cr·**4**·apo-H64D/A71GMb: Yield 22%, ESI-TOF MS: 17 697.0 (calcd 17 696.1), UV−vis (10 mM Tris/HCl buffer, pH 7.0) λ/nm (ϵ/M^{-1} cm^{-1}): 282.5 (61 950), 346.0 (9050) sh, 419.0 (5550). Cr·**1**·apo-A71GMb: Yield 9%, ESI-TOF MS: 17 709.6 (calcd 17 710.1), UV−vis (10 mM Tris/HCl buffer, pH 7.0) λ/nm (ϵ/M^{-1} cm^{-1}): 281 (34 200), 345 (26 000), 481 (9500).

Physical Measurements. UV−vis spectra were recorded on a Shimadzu UV-2400PC UV−vis spectrophotometer. ^{1}H NMR spectra were recorded on a JEOL JNM-L 500 NMR spectrometer. ESI-TOF mass spectra were measured on an LCT (Micromass, U.K.). Typical parameters were capillary: 3 kV; cone: 60 V; source temperature: 60 °C; flow-rate: 5 μL min^{-1}; and mass scale calibration: CsI (1 mg/ mL) in 50% H$_2$O/CH$_3$CN. All samples were dialyzed against 5 mM ammonium acetate for 8−10 h at 4 °C. The concentrations of Mn and Cr ions in the reconstituted enzymes were determined by using a polarizing Zeeman-effect atomic absorption spectrophotometer Z-5710 (HITACHI) operating in graphite furnace mode using a Mn or Cr hollow cathode lamp. Mn(NO$_3$)$_2$ in 0.1 mol/L·HNO$_3$ (100.5 mg/L) and K$_2$Cr$_2$O$_7$ in 0.1 mol/L·HNO$_3$ (100.3 mg/L) were used as calibration standards.

Catalytic Sulfoxidation. Sulfoxidation was carried out in sodium acetate buffer (50 mM, pH 5.0) at 35 °C. The reaction mixture contained 10 μM Mb complex, 1 mM H$_2$O$_2$, and 1 mM thioanisole. Acetophenone was added as an internal standard, and the mixture was extracted with dichloromethane for HPLC analysis on a Daicel Chiralcel OD column installed on a Shimadzu SPD-10A spectrophotometer equipped with a Shimadzu LC-10AD pump system.[50] At least two experiments were performed for each experimental point.

Sulfoxides were synthesized from the corresponding starting substrates by the oxidation with *m*-chloroperbenzoic acid and used to make standard curves.

Crystallization, X-ray Data Collection, and Crystallographic Refinement. The crystallizations of Cr·**1**·apo-A71GMb and Mn·**1**·apo-A71GMb were carried out as described previously.[30] Cr·**1**·apo-A71GMb was purified by CM52 and RESOURCE S and crystallized at 4 °C with a hanging-drop vapor diffusion method. Drops of 6 μL containing approximately 7.7 mg/mL protein and sodium/potassium−phosphate buffer (NaH$_2$PO$_4$/K$_2$HPO$_4$, pH 6.8, 1.4 mol/l) were equilibrated against a 1000 μL reservoir solution containing the same buffer in 2-fold higher concentration (2.8 mol/L). Orange crystals grew within a week (2.0 × 0.15 × 0.11 mm^3).

Mn·**1**·apo-A71GMb was purified with Sephadex G-75 on an AKTA explorer 100 FPLC system (Amersham Biosciences) and crystallized at 4 °C with the hanging-drop vapor diffusion method. Drops of 6 μL containing approximately 8.7 mg/mL protein and sodium/potassium− phosphate buffer (pH 6.8, 1.4 M) were equilibrated against 1000 μL reservoir solution containing the same buffer in 2-fold higher concentration (2.8 M). The brown crystals grew within two weeks (0.85 × ∼0.15 × ∼0.12 mm^3).

Before data collection, the crystal of Cr·**1**·apo-A71GMb was briefly immersed in a cryoprotectant solution that consisted of 15% (w/v) glycerol and 2.8 M sodium/potassium−phosphate buffer (NaH$_2$PO$_4$/ K$_2$HPO$_4$, pH 6.8). X-ray diffraction data were collected at 100 K using

Rigaku FR-E X-ray generator (wavelength: 1.5418 Å, Cu Kα) and R-AXIS VII detector at the High-Intensity X-ray Laboratory, Nagoya University. The data were processed with the programs *Denzo* and *Scalepack* (completeness: 97.1%, R_{merge}: 9.3% for all data up to 1.45 Å resolution).[51] The crystal belongs to the space group $P2_12_12_1$, with unit cell dimensions $a = 33.0$ Å, $b = 58.8$ Å, and $c = 76.2$ Å, and contains one composite in an asymmetric unit.

As the initial model for the refinement, biliverdin·apo−Mb complex (PDB code 1BVC) was used without biliverdin. After a few cycles of refinement, the resulting electron-density map allowed the fitting of Cr·**1** model bound to His93 residue in the heme cavity. The structure model was manually corrected with the TURBO-FRODO program and recurrently refined with *CNS*[52] to the final *R*-factor and the R_{free} values of 19.4 and 21.9%, respectively. The final model contained Cr·**1**, six phosphate ions, and 152 residues, but excluded Lys96 and His97 due to their disordered electron density. The model was subjected to quality analysis during the various refinement stages with omit maps and PROCHECK.[39] All residues (residue numbers: 0−95 and 98−153) in the final model fell into either the most favored or additionally allowed regions of the Ramachandran plot.

The Cr·**1**·apo-A71GMb structure with deletion of the Cr·**1** moiety was used as an initial model for the refinement of Mn·**1**·apo-A71GMb. The refinement was carried out with the program *CNS*, and manual model building was carried out with the program TURBO-FRODO. A statistically random selection of about 5% of the total reflection data was excluded from the refinement and used to calculate the free *R* factor (R_{free}) as a monitor of model bias. After rigid-body refinement, positional refinement, and *B*-factor refinement, Mn·**1** was positioned manually on omit $|F_o| - |F_c|$ map in the heme cavity. Several subsequent cycles of refinement brought the final *R* factor and the R_{free} value to 20.6 and 21.8%, respectively. The model was subjected to quality analysis during the various refinement stages with omit maps and PROCHECK. The crystal parameters and data collection statistics are given in Table 1.

The coordinates of the Cr·**1**·apo-A71GMb and Mn·**1**·apo-A71GMb have been deposited in the Protein Data Bank, under accession numbers 1J3F and 1V9Q, respectively. These data can be obtained free of charge via the Protein Data Bank (http://www.rcsb.org/pdb/).

Molecular Modeling. Energy minimization calculations of Mn·**2**· apo-H64D/A71GMb, Mn·**3**·apo-H64D/A71GMb, Mn·**4**·apo-H64D/ A71GMb were performed using InsightII 2000/Discover 3 with the Extensible Systematic Force Field (ESFF) Forcefield (Accelrys Inc.). The initial structures were generated by replacing His64 and **1** of Mn· **1**·apo-A71GMb (PDB: 1V9Q) with Asp and **2**, respectively. The residues out of 10 Å from the Mn atom were fixed during the calculations. Mn·**3**·apo-H64D/A71GMb and Mn·**4**·apo-H64D/A71GMb were calculated by the same protocol.

(50) Ozaki, S.; Yang, H.-J.; Matsui, T.; Goto, Y.; Watanabe, Y. *Tetrahedron: Asymmetry* **1999**, *10*, 183−192.
(51) Otwinowski, Z.; Minor, W. *Methods Enzymol.* **1997**, *276*, 307−326.
(52) Brunger, A. T.; Adams, P. D.; Clore, G. M.; DeLano, W. L.; Gros, P.; Grosse-Kunstleve, R. W.; Jiang, J. S.; Kuszewski, J.; Nilges, M.; Pannu, N. S.; Read, R. J.; Rice, L. M.; Simonson, T.; Warren, G. L. *Acta Crystallogr. D* **1998**, *54*, 905−921.